*Meteoritics & Planetary Science* 43, Nr 4, 701–716 (2008)
Abstract available online at http://meteoritics.org

# Structural evolution of the 40 km wide Araguainha impact structure, central Brazil

C. LANA[1*], C. R. SOUZA FILHO[2], Y. R. MARANGONI[3], E. YOKOYAMA[3], R. I. F. TRINDADE[3], E. TOHVER[4], and W. U. REIMOLD[5]

[1]Department of Geology, University of Stellenbosch, Private Bag X1, Matieland 7620, South Africa
[2]Departamento de Geologia e Recursos Naturais, Instituto de Geociencias, UNICAMP, 13083-970 Brazil
[3]Instituto de Astronomia, Geofísica e Ciencias Atmosfericas, USP Rua do Matao,1226, Cidade Universitaria, São Paulo, SP 05508-090, Brazil
[4]Tectonics Special Research Center, University of Western Australia, 35 Stirling Highway, Crawley, WA 6009, Australia
[5]Museum for Natural History (Mineralogy), Humboldt University, Invalidenstrasse 43, 10115 Berlin, Germany
[*]Corresponding author. E-mail: lana@sun.ac.za

*(Received 29 March 2007; revision accepted 05 September 2007)*

**Abstract**–The 40 km wide Araguainha structure in central Brazil is a shallowly eroded impact crater that presents unique insights into the final stages of complex crater formation. The dominant structural features preserved at Araguainha relate directly to the centripetal movement of the target rocks during the collapse of the transient cavity. Slumping of the transient cavity walls resulted in inward-verging inclined folds and a km-scale anticline in the outer ring of the structure. The folding stage was followed by radial and concentric faulting, with downward displacement of kilometer-scale blocks around the crater rim. The central uplift records evidence for km-scale upward movement of crystalline basement rocks from the transient cavity floor, and lateral moment of sedimentary target rocks detached from the cavity walls. Much of the structural grain in the central uplift relates to structural stacking of km-scale thrust sheets of sedimentary strata onto the core of crystalline basement rocks. Outward-plunging radial folds indicate tangential oblate shortening of the strata during the imbrication of the thrust sheets. Each individual sheet records an early stage of folding and thickening due to non-coaxial strains, shortly before sheet imbrication. We attribute this folding and thickening phase to the kilometer-scale inward movement of the target strata from the transient cavity walls to the central uplift. The outer parts of the central uplift record additional outward movement of the target rocks, possibly related to the collapse of the central uplift. An inner ring structure at 10–12 km from the crater center marks the extent of the deformation related to the outward movement of the target rocks.

## INTRODUCTION

Early studies by Dence et al. (1968), Hartmann (1972), and Pike (1974, 1977, 1983) have long indicated that the morphological and morphometric characteristics of meteorite impact craters vary as a function of size. Terrestrial impact structures, for example, have been shown to change from a simple bowl-shaped crater to a more complex structure (a central-peak crater) at diameters between 2 and 4 km (Dence et al. 1968; Grieve et al. 1981; Grieve 1987). With continued increase in crater diameter, complex structures may change internally, whereby their central peak is replaced by a concentric peak ring. However, the internal geometry of large (>25 km) impact structures remains a matter of contentious debate, as an increasing number of field-based mapping and geophysical experiments indicate that terrestrial craters of similar sizes may have distinct internal structures and morphologies (Jansa et al. 1989; Tsikalas et al. 1998a, 1998b; Morgan et al. 2000; Dypvik and Jansa 2003; Grieve and Therriault 2000, 2004; Vermeesch and Morgan 2004; Wünnemann et al. 2005). The structural variation between terrestrial craters seems to be a result of the distinct response of different target rocks (under distinct strain regimes and geothermal gradients) to the extreme pressure and temperatures released upon impact (Ivanov and Deutsch 1999; Lana et al. 2003a, 2003b, 2006a, 2006b; Spray et al. 2004; Dence 2004; Collins et al. 2004; Gibson and Reimold 2005; Riller 2005).

In an effort to shed some light onto the internal structure of large terrestrial craters we call attention to an underappreciated and poorly studied impact structure in central Brazil. The 40 km wide Araguainha impact structure is a rare example of a shallowly eroded impact structure that provides an unparalleled opportunity to study the kinematics of complex crater formation (Fig. 1) (Crósta et al. 1981;

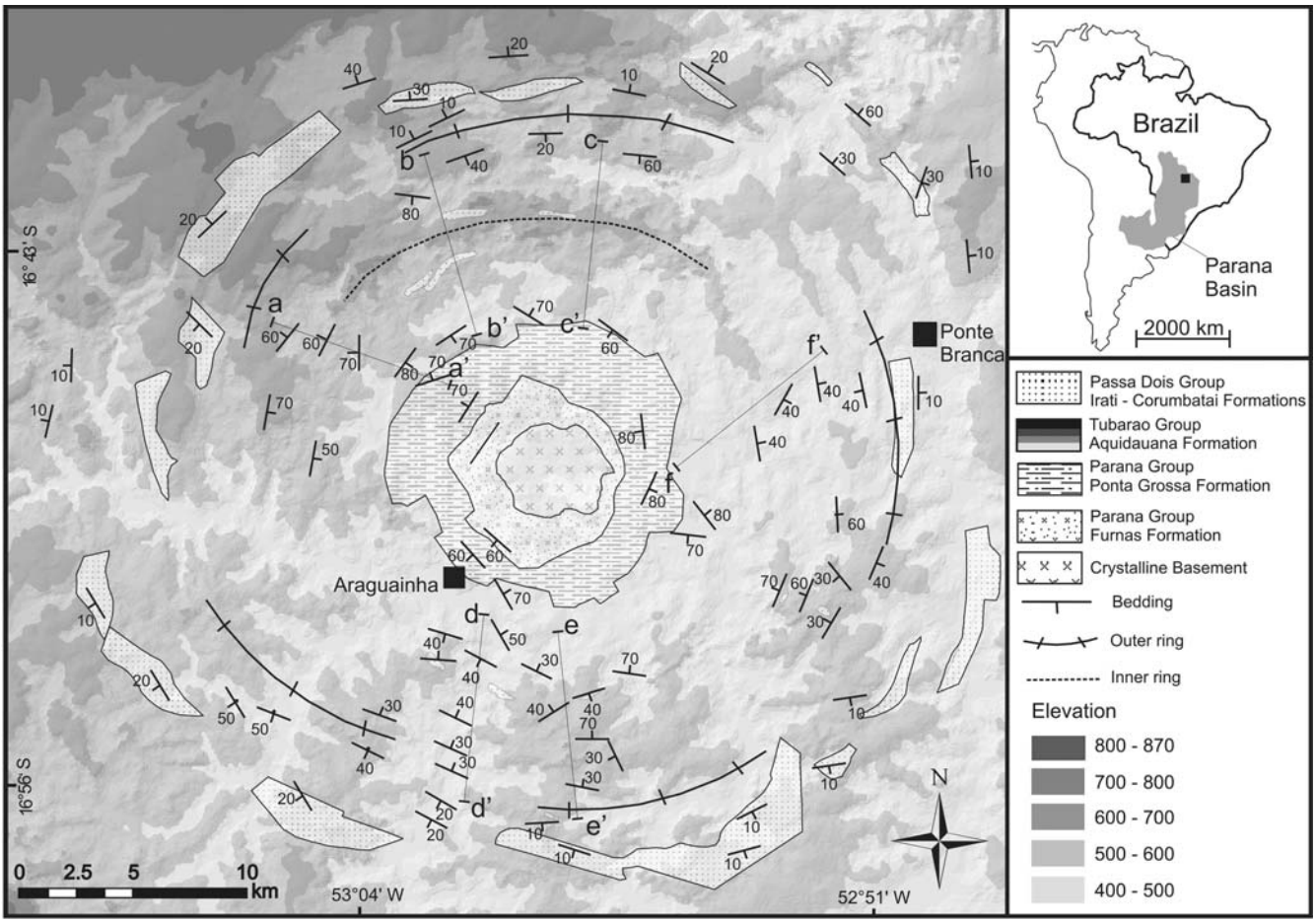


Fig. 1. Geological map of the Araguainha impact structure, showing the main lithological units and bedding orientations. The image in the background is a triangular irregular network (TIN) surface converted from ASTER digital elevation. Note that the TIN surface depicts well the outer and inner topographic concentric rings described by Lana et al. (2007) (see text for more details). The bars labeled a-a' to f-f' represent structural profiles analyzed for the inner ring feature: the structural data are presented in stereoplots of Fig. 5b.

Theilen-Willige 1981; Engelhardt et al. 1992; Lana et al. 2006a, 2007). Remote sensing analysis and stratigraphic correlations indicate that Araguainha preserves a fully exposed central peak, an annular basin and two main concentric ring features (Fig. 2a) (Lana et al. 2007). The crater rim is also well exposed, providing important insights into the mechanics of crater rim collapse (Fig. 2a). Lana et al. (2007) have demonstrated that the present morphology of the crater is largely controlled by the concentric arrangement of the structures and layered sedimentary units. However, while some structural data have been reported for some parts of the impact structure (Lana et al. 2006a, 2007), no comprehensive structural analyses have been directed at understanding the geometry of the central uplift and the crater rim. In addition, the structural implications of the concentric ring features for the evolution of the impact crater have not been fully discussed. In this contribution, we expand the structural data set available for Araguainha and present a detailed structural analysis of the entire impact structure (Fig. 1). Thematic Mapper (TM) (Fig. 2a) and Advance Spaceborne Thermal Emission and Reflection Radiometer (ASTER) data are combined with the structural inventory to provide a direct correlation between the morphological and structural features. The objective is to establish the nature of strain that led to formation of the central uplift, concentric rings, and the crater rim.

## GEOLOGY OF ARAGUAINHA

The Araguainha impact structure is the eroded remnant of the largest impact crater in South America (Crósta et al. 1981; Theilen-Willige 1981; Engelhardt et al. 1992; Lana et al. 2006a, 2007). It is located in the northeastern part of the Paraná Basin (Fig. 1), straddling the border between Mato Grosso and Goias states in central Brazil. Previous studies in and around the impact structure have indicated that the target rocks comprise relatively well exposed Devonian to Permo-Triassic sediments of the Paraná Basin and underlying crystalline basement rocks of the Braziliano Shield (Silveira Filho and Ribeiro 1973; Pena 1974; Crósta et al.

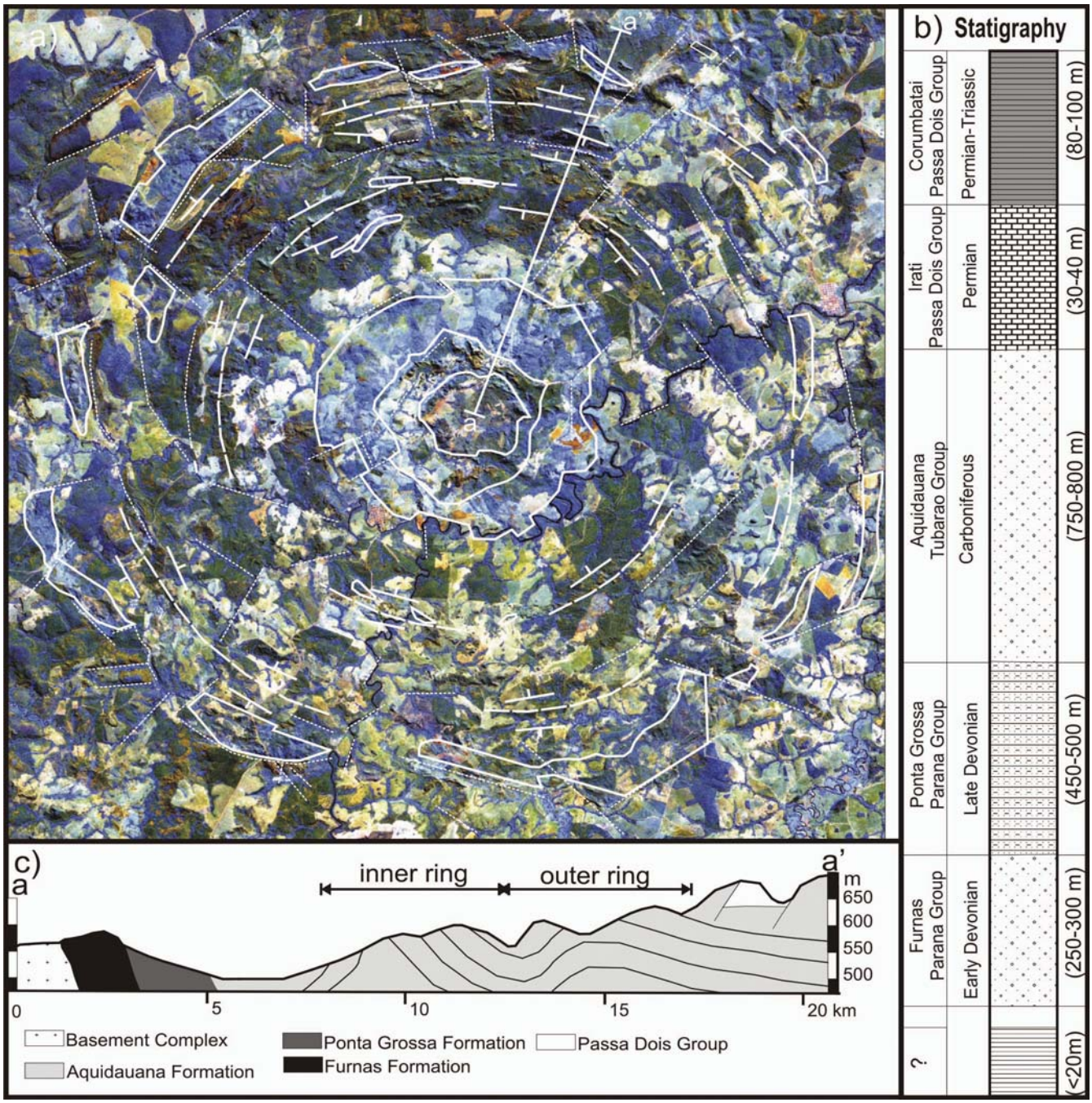


Fig. 2. a) Main structural lineaments (short-dashed lines) and lithological contacts (solid lines) overlapped with false color composite image of Landsat TM displayed in RGB. Contours of the inner and outer ring features (long-dashed lines) are also shown. b) Simplified stratigraphic column of the Araguainha target rocks (after Lana et al. 2007). c) Profile showing lithologies and an interpretation of a 2D geometry of the inner and outer ring features. Extent and orientation of the profile is labeled in Fig. 2a.

1981; Theilen-Willige 1981; Engelhardt et al. 1992; Bischoff and Prinz 1994; Hammerschmidt and Engelhardt 1995). The target rocks inside the structure belong to the Passa Dois, Tubarão and Paraná Groups (Fig. 2b). The Passa Dois Group comprises 20–40 m thick Permian siltstone, chert and carbonate (Iratí Formation) and 80–100 m thick Permian-Triassic siltstones and subsidiary sandstones and chert (Corumbataí Formation). The Tubarão Group is represented by a 700–800 m thick section of Carboniferous sandstones and conglomerates, overlain by stratified siltstones and sandstones (Aquidauana Formation). The Paraná Group encompasses 800 m thick Devonian fluvial white sandstones and conglomerates (Furnas Formation) and marine siltstones and minor sandstones (Ponta Grossa Formation)

(Fig. 2b). The underlying crystalline basement consists of porphyritic granitic rocks with xenoliths of metamorphosed sandstones and siltstones. Although these target rocks have been variably deformed during the impact event, the same sedimentary strata outside the impact crater retain their original horizontal sedimentary layering and do not record evidence of pre- or post-impact deformation (Silveira Filho and Ribeiro 1973; Pena 1974; Lana et al. 2007).

Many of the macroscopic features diagnostic of impacts such as shatter cones, impact melt rocks, and polymict and monomict breccia deposits are preserved in the central parts of the structure (Crósta et al. 1981; Theilen-Willige 1981; Engelhardt et al. 1992). The impact melt and breccias are found as relatively thin blankets covering the core and collar of the central peak. Previous petrographic observations by Engelhardt et al. (1992) have provided important evidence that the polymict breccias contain partly molten, slightly contorted clasts of the Paraná sedimentary sequence. Other clasts have been described as shocked, partly molten granites and hornfels that derived from excavation of the crystalline basement below the Paraná strata (Engelhardt et al. 1992). Petrographic studies by Engelhardt et al. (1992) led to the conclusion that energy released upon the impact was sufficient to excavate a 2–2.5 km vertical section through the undeformed sediments of the Paraná Basin and part of the underlying crystalline basement rocks (Fig. 2b) (see also, Lana et al. 2006a, 2007). The excavation of the Paraná sediments affected an area with a radius of several kilometers and resulted in a 20–25 km wide cavity with a minimum depth of 2–2.5 km (Lana et al. 2006a). Gravitational collapse of the excavated crater led to structural uplift of the Ordovician to Permo-Triassic sediments around a 5 km wide core of crystalline basement rocks in the center of the structure (Figs. 1 and 2c) (Crósta et al. 1981; Theilen-Willige 1981; Bischoff and Prinz 1994).

Detailed stratigraphic analysis has demonstrated that the structure experienced two main periods of erosion since the impact event. However, while erosion was sufficient to remove most of the impact-related deposits (impact breccias and impact melt layer), the floor of the structure remained relatively well preserved, with the typical concentric geometry of a large impact crater (Romano et al. 2006; Lana et al. 2007). The most noticeable morphological features shown by ASTER digital elevation model include a 6–7 km wide central peak, surrounded by a 5 km wide annular basin and two main concentric ring features at 10–12 km and 14–18 km from the center of the structure (Figs. 1a and 2a) (Lana et al. 2007). The inner ring comprises a major topographic feature that stands some 200 meters higher than the floor of the annular basin (see elevation data in Fig. 1). The outer ring is bordered by several radial and ring faults that define the rim of the structure (Figs. 1a and 2a).

Concentric features have also been suggested to occur in the crystalline rocks below the sedimentary target sequence (Masero et al. 1994; Schnegg and Fontes 2002). One-dimensional modeling of magnetotelluric (MT) data indicated to Massero et al. (1994) that target rocks at 3–7 km below surface were affected by concentric and radial faults/fractures over a 16 km-diameter area. According to their study, the basement rocks may form a 12–16 km diameter ring feature that surrounds a 6 km wide central peak. Further refinements to this model led Schnegg and Fontes (2002) to suggest that the central peak is surrounded by an annular basin and two main concentric rings. In addition, Schnegg and Fontes (2002) study also indicates that the annular basin becomes progressively deeper outwards, reaching a maximum depth of ~3 km at ~11 km from the center. Although the MT data modeling was hampered by poor MT coverage, the results obtained by Masero et al. (1994) and Schnegg and Fontes (2002) seem to indicate that the concentric morphological and structural features observed at surface (Lana et al. 2007) have been deeply carved into the basement rocks, at 2 km below surface.

## CRATER RIM AREA

The crater rim at Araguainha is characterized by kilometer-scale blocks of variably deformed Passa Dois and Aquidauana sediments (Figs. 1a and 1b). Our Landsat TM and ASTER imagery data show clearly the geometry of the several blocks of the Passa Dois Group (Figs. 2a, 3a, and 3b). This is because the Passa Dois Group is characterized by a coarser texture and more uniform tonal variation relative to the Aquidauana Formation, making it easier to define the lithological contacts. Our field based mapping and remote sensing analysis indicate that several of the km-scale blocks have an arcuate geometry (Figs. 2a, 3a, and 3b), consistent with their concentric arrangement around the crater rim. This geometry is largely controlled by the geometry of the faults, in addition to km-scale folding and localized brecciation of the strata.

### Folding

The present structural data set for the crater rim indicates that the overall bedding orientation of the Passa Dois Group is subhorizontal, shallowly dipping toward the crater rim (Fig. 1). While this seems consistent with the geometry of terraced walls in generic models for terrestrial craters (e.g., Grieve et al. 1981; Grieve 1987), we observed that the bedding orientation in the largest blocks of the Passa Dois (in the southwest, northwest, and southeast) may show localized variations due to shallow (gentle) folding of the strata on a hundred-meter scale (Fig. 3c). The hinge lines of these open folds are invariably subhorizontal, with an orientation that is preferentially radial or tangential to the main circular geometry of the crater rim (Fig. 3c). The same seems to apply for the bedding in the Aquidauana Formation, which is slightly buckled, dipping shallowly (5°–10°) inwards and outwards (e.g., Lana et al. 2006a). The geometry

of the folds is consistent with large-scale, layer parallel shortening of the Passa Dois and Aquidauana sediments during the downfaulting of the individual fault-bounded blocks.

The large-scale folding of the target sediments was accompanied by localized development of outcrop-scale folds in the Passa Dois Group. Many of these small-scale folds have been identified in the southern and western parts of the crater, where the Passa Dois Group bedding is folded into open to tight recumbent folds with shallowly plunging hinges (Fig. 3d). The fold hinges range from oblique to tangential with respect to the circular geometry of the crater rim. Small-scale intrafolial folds are also present (Fig. 3e). The geometry of these folds is consistent with a strong component of non-coaxial deformation, associated with the inward movement of the Passa Dois sediments towards the center of the crater (see also Lana et al. 2006a). Local variation of bedding and fold hinges is observed near the radial faults, whereby bedding orientation changes from concentric (dipping shallowly inwards and outwards) to radial (parallel to the fault planes). In this case, refolding of the pre-existing structures occurred contemporaneously with motion along the radial faults (discussed below).

**Faulting**

Fault zones are very prominent structural features along the crater rim (Figs. 1a and 2a). They vary from a few centimeters to several meters in width, and are often associated with conjugate sets of fractures, which are oriented orthogonally to the main fault plane. In most cases, the master plane of the fault zones is generally defined by a curved or planar, cm-wide surface: however, the planes themselves are seldom exposed and cannot always be traced at an outcrop scale. Analysis of the orientation and distribution of these fault zones has only been possible with combined structural observations and remote sensing imagery (Figs. 2a, 3a, and 3b).

Our remote sensing analysis allows a clear definition of the trace of the faults in all sectors of the Araguainha structure (e.g., Fig. 2a). The analysis was applied to the fault planes located in steep and straight gullies that cut across the Aquidauana and Passa Dois sediments. The dominant fault set comprises concentrically arranged, brittle zones that juxtapose the Passa Dois with the Aquidauana sediments. The outermost fault zones (defining the crater rim: Figs. 1c, 2a, and 2b) have been observed near steep escarpments of the Aquidauana sandstones, which locally stand from 10 to 30 m above the crater floor (Fig. 4a). The fault planes are vertical to steeply dipping towards the center of the structure. Their curvature cannot be constrained with the present data set, although it is clear from the Landsat TM and ASTER imagery that the contact between the sediments is concentric with respect to the center of the structure (Figs. 3a, 3b, and 4b). The vertical displacements along the concentric fault zones range from 200 to 300 m (Lana et al. 2006a). In the southwestern sector, where sediments are well exposed along road cuts, the vertical displacement between the Iratí sediments (Ponta Grossa Group) has been measured at approximately 250 m (e.g., Fig. 1c) (Lana et al. 2007).

A second set of fault zones includes those that are radial to oblique to the main circumference of the crater rim. The oblique trending faults are the most easily depicted (Fig. 4c). They form conjugate pairs that separate triangular- or diamond-shaped wedges of the Aquidauana sandstones (Figs. 4b and 4c). Some of the faults extend from the crater rim to the annular trough and displace several large-scale structures, including the concentric ring features (e.g., Figs. 2a and 5a; described below). In this case, the concentric ring features have been separated into several km-scale arc segments that have been displaced inwards or outwards (Fig. 2a). The largest displacement is observed in the northern and northwestern sectors where the outer anticline and the crater rim have been displaced by 1–2 km (Fig. 5a). Here, the arrangement of the blocks suggests that the radial faults also accommodated hundreds of meters to several kilometers of lateral movement (Figs. 2a and 5a). Rare shallowly plunging slickensides and grooves in the fault planes indicate oblique movement, with a strong strike-slip component between the various blocks of the Aquidauana Group.

Several of the radial faults extend up to 2–10 km outside the crater rim, where relatively undeformed sediments of the Passa Dois Group (exposed to the west, south and southwest of the crater rim) have been juxtaposed with the Aquidauana sediments. For example, a NE-trending reverse fault has a measured vertical throw of 4 meters and juxtaposes the Ponta Grossa with the Aquidauana (Figs. 4d and 4e). The main reverse fault plane is associated with small normal faults (Fig. 4e). These faults record, however, small displacements and cannot be related to collapse of the crater rim: they rather reflect block adjustments or reactivation of pre-existing faults in the crystalline basement.

The trace of the major lineaments observed on the Landsat TM and ASTER images from the northern and northwestern sectors (Figs. 3a and 3b) suggest that the concentric faults are intersected by radial or oblique faults. However, there are several sets of small radial faults that do not offset the concentric faults at the contact between the Passa Dois Group and Aquidauana Formation (Figs. 3a, 3b, and 4b). This is evident in the southwestern sector where a number of NE-trending faults are truncated by a concentric fault at the Aquidauana Formation—Passa Dois Group contact (Fig. 4b). It is not clear whether the radial and concentric faults formed at distinct stages of the cratering process, even though the faults themselves have distinct geometries.

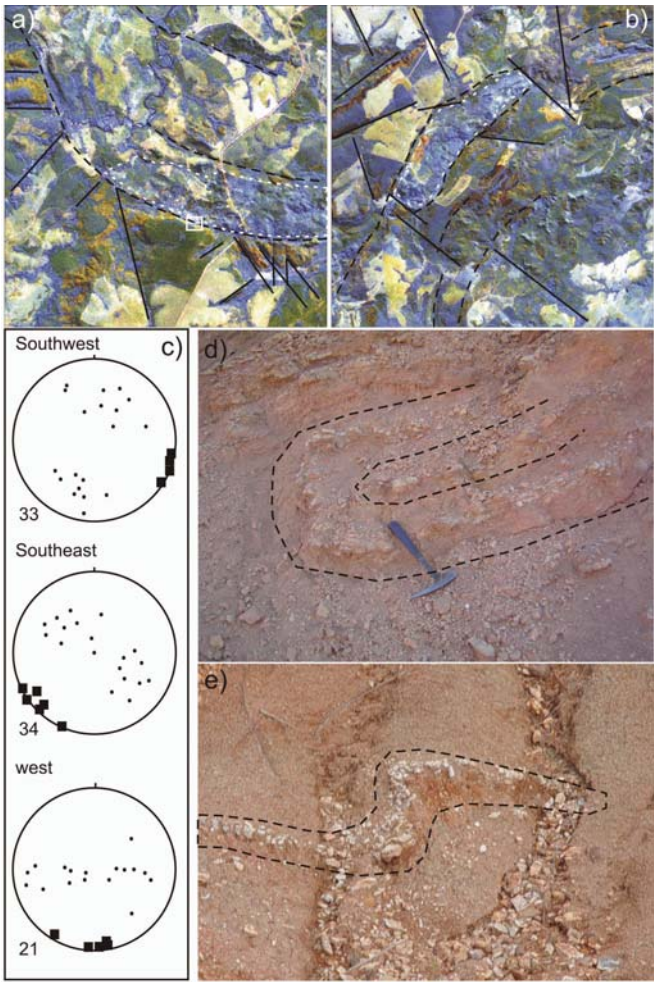


Fig. 3. a–b) Landsat TM images of the crater rim showing km-scale blocks in the southwestern (a) and northwestern (b) sectors. Dashed white lines mark the lithological boundaries between Aquidauana sandstones and Passa Dois siltstones. Dashed black lines mark the concentric faults of the crater rim. Solid black lines indicate the main trend of the radial faults. c) Low hemisphere equal area stereonet projections of the folded bedding (full circles) at the crater rim. Dotted lines mark the inferred hinges of the gentle folds (see text for details). d–e) examples of outcrop-scale asymmetric folds in the Passa Dois Group in the southwestern (d) and southeastern (e) sectors.

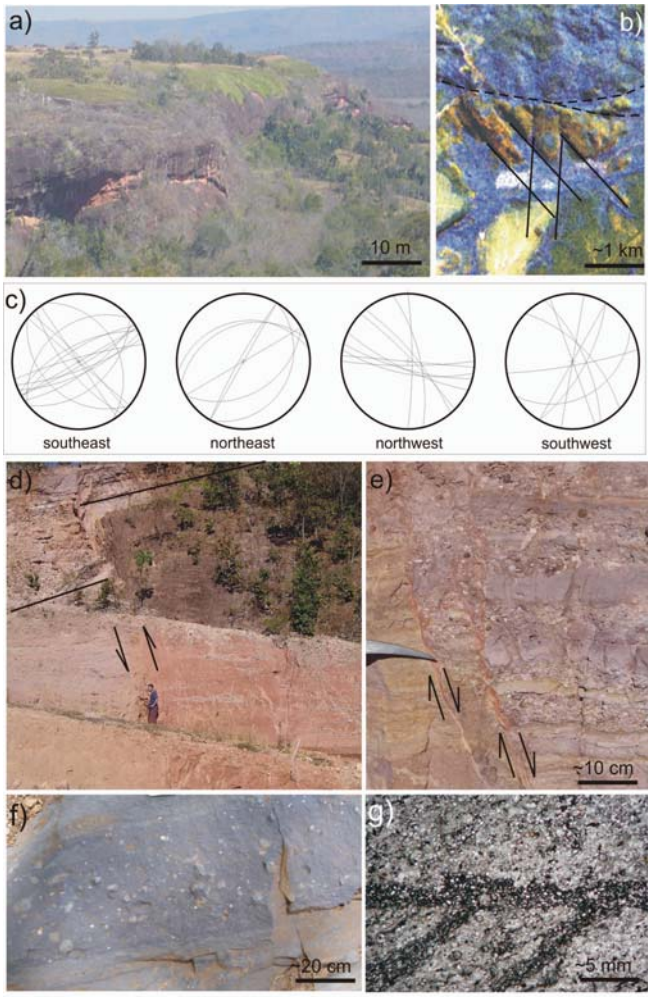


Fig. 4. a) Overview of the Aquidauana sandstones forming a major escarpment at the crater rim (southwestern sector). Location of the photograph is marked by white box in Fig. 3a. b) Conjugate sets of oblique faults in the southwestern sector. The faults separate blocks of the Aquidauana sediments on a hundred-meter scale. c) Lower hemisphere equal area stereonet projections of faults at the crater rim. d) Large-scale radial reverse fault juxtaposing the Passa Dois and Aquidauana sediments. The contact between the sediments is marked by solid line. e) Secondary normal faults associated with the reverse fault shown in (d). The faults displace the sediments on a centimeter scale. e) Dike of breccia cross-cutting the Passa Dois sediments. f) Millimeter-scale breccia vein in the Passa Dois sediments. The main vein (horizontal) is parallel to the bedding of the Passa Dois siltstone and is interconnected with a number of oblique veins.

## Local-Scale Brecciation of the Crater Rim Sediments

Brecciation of the target rocks inside the crater rim area is expressed in the form of mm-wide veins to meter-wide dykes of cataclastic breccias. The dykes are characterized by poorly sorted angular to rounded clasts, surrounded by a fine-grained to cryptocrystalline groundmass (Figs. 4f and 4g). The clasts comprise either rock or mineral fragments of the host rock, ranging in size from a few mm to several cm. The mm-scale breccia veins are often observed near the dykes and occur in close association with a network of mm-scale fractures. The veins consist dominantly of mineral fragments in a cryptocrystalline black matrix (Fig. 4g). The mineral fragments (e.g., quartz and feldspar) have been largely fractured during brecciation.

The breccia dykes vary in attitude from horizontal to vertical and have no preferred orientation with respect to the impact-related faults. Even though they occur inside the crater rim (very often near the contact with the Aquidauana sediments), their temporal relationship with the radial or concentric faults has not been observed. On the other hand,

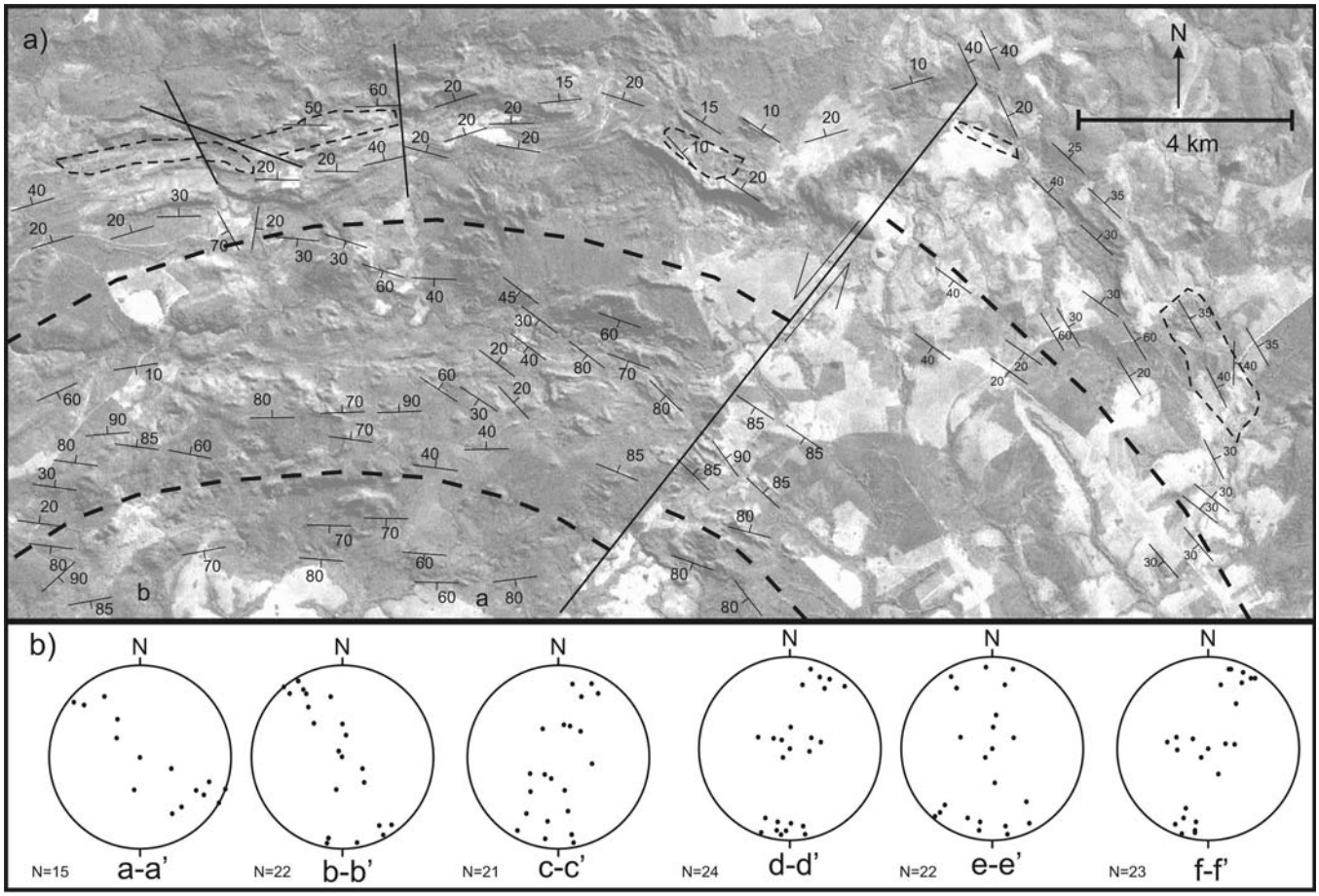


Fig. 5. a) Structural data for the northern and northwestern sectors of the crater. Solid lines represent the main fault zones displacing the crater rim and the ring features. The contours of the inner and outer rings are marked with thick dashed lines. Thin dashed lines highlight the lithological boundaries at the crater rim. b) Lower hemisphere equal area stereonet projections of the rotated strata (full circles) in the inner ring feature: the structural data were collected along several profiles as indicated in Fig. 1.

both dykes and veins cross-cut dominantly local-scale folds in the Passa Dois and Aquidauana rocks. Much of the millimeter-wide veins and fracture networks are predominantly subparallel to the folded bedding planes and displace the bedding on a millimeter scale. Opposite sense of displacements are commonly observed in the same outcrop, as if the strata oscillated during the development of the millimeter-wide crush zones.

## CONCENTRIC RING FEATURES

Structural and remote sensing observations suggest that the annular ring area comprises two main ring features at 10–12 km and 14–18 km from the center of the structure (Lana et al. 2007). The rings are expressed in the form of ridges or aligned hills that surround the annular basin (Fig. 2a). Bedding orientations collected throughout the northern sector (Fig. 5a) and along 6 main profiles (a-a' to f-f'; Fig. 1) indicate a concentric geometry for both ring features (Fig. 5b). The outer ring has been segmented by several of the radial faults (Figs. 1a and 2a). The segments (as well as the blocks of the Passa Dois Group in the crater rim area) have been laterally dislocated by 500 m to 2 km. The inner ring has also been affected by radial (or oblique) faults, but it does not record large-scale lateral displacements. It is possible that the lateral displacements decrease in magnitude towards the center of the crater; a feature consistent with the severe space problems expected to occur in the central parts of the crater (Melosh 1989; Melosh and Ivanov 1998; Shoemaker and Shoemaker 1996; Milton et al. 1996; Ivanov and Deutsch 1999; Kenkmann and Dalwigk 2000).

The geometry of the outer ring has been well constrained in the northern and northwestern sectors (Figs. 5a and 5b), where the majority of outcrops are of the bedded siltstones of the upper Aquidauana Formation. Our present structural data set for this sector indicates an inward-verging antiformal geometry for the outer ring, with a relatively shallow outer limb (dipping at 10°–20° outward) and a relatively steep inner limb (dipping at 40°–60° inward). The core of the antiform is characterized by subhorizontal to shallowly folded bedding orientations, indicating a horizontal to shallowly plunging hinge. The geometry of the inner ring feature is complex. In

the northern part of the inner ring, the Aquidauana bedding dips steeply (50°–80°) inwards or outwards, suggesting an upright antiformal geometry (Figs. 5a and 5b). For the rest of the inner ring, however, the sandstones are largely faulted, and generally poorly exposed. The variation in bedding orientation may be related to tilting of meter- to hundreds-of-meters-scale blocks, as revealed by seismic profiles across impact craters of similar size (Jansa et al. 1989; Tisicalas et al. 1998). The bulk of the structural measurements suggests that the inner ring is either an upright tight anticline or a steeply dipping monocline. Several upright to recumbent parasitic folds, with horizontal to shallow, doubly plunging hinge lines are observed. The folds range in scale from meters to tens of meters wide, but are only partially preserved or poorly exposed (e.g., Lana et al. 2006a). The hinges are parallel to the main concentric arrangement of the anticline axis.

The main structure separating the two ring features cannot be characterized at present because of difficult access to the main outcrops in the northern and western sector, and the overall lack of exposure in the southern half of the crater. Bedding orientations between the anticlines suggest a relatively tight syncline with both parasitic folding and local-scale faulting, most clearly evident near the contact with remnants of the Passa Dois Group, 10–15 km from the central uplift. The Passa Dois Group was juxtaposed with the sandstones of the Aquidauana Formation along radial and concentric faults. The presence of densely spaced fracture-network and breccias veins and dykes in the Passa Dois sediments suggest that faulting was associated with local-scale brecciation.

## THE CRATER CENTER

The central part of the Araguainha structure is characterized by two distinct morphological features that have been described by Lana et al. (2007) as a 6–7 km wide central peak and a 5 km wide annular basin (Fig. 2a). The central peak is a major structural high that consists of a 4–5 km wide core of porphyritic granite and a 1–2 km wide collar of upright to overturned sediments of the Furnas Formation (Figs. 1a and 2a). The surrounding annular basin is a flat circular depression between the concentric rings and the central peak. The basin exposes sediments of the uplifted Ponta Grossa Formation and the highly fractured sandstones of the Aquidauana Formation. As noted previously (Lana et al. 2007), the central peak is a morphological feature and does not entirely correspond to the central uplift of the structure. The minimum extent of uplifted rocks in the central part of the crater is indicated by the Ponta Grossa-Aquidauana contact, located at 10–12 km from the center of the crater (Figs. 1a and 2a). According to borehole core and stratigraphic information the Ponta Grossa-Aquidauana contact was >900 m below the surface prior to the impact event. The maximum uplift of this contact and the overlying sediments cannot yet be constrained, because the basal Aquidauana sandstones do not contain well defined stratigraphic markers. Nevertheless, it is clear from our stratigraphic data that the Aquidauana basal sediments were uplifted by at least hundreds of meters during the formation of the central uplift. This implies that the diameter of the central uplift is substantially larger than previously proposed (e.g., 10 km; Lana et al. 2006a), encompassing much of the central peak and annular basin.

### The Central Peak

Although several Landsat images show a symmetric, circular geometry for the central peak at Araguainha, our field-based observations indicate a rather asymmetric distribution of the collar sediments around the granite core (Fig. 6a). The central peak displays an off-centered polygonal geometry, with the Furnas Formation being substantially thinner in the northeastern and southeastern sectors relative to the northwestern and southwestern sectors (Fig. 6a). This asymmetric distribution of the sediments relates directly to differential thickening of the strata in each sector of the central uplift. Given the subvertical orientation of the collar strata and the original thickness of the Furnas sediments (300 m outside the structure), it is possible that the formation has been thickened by a factor of 2 in the southeastern sector and a factor of 7 in the northern and northwestern sectors. The thickening of the Furnas sequence is the result of several processes (thrusting, imbrication of strata, and folding) that contributed to the formation of the central uplift (described below).

The inner part of the collar comprises a 500 m wide complex zone of meter- to hundreds of meter-scale blocks of basal sediments of the Furnas Formation. The blocks were tilted at various degrees during the structural arrangement of the sediments around the granitic core. Well exposed sections across the collar-core contact indicate that the basal sequence of the Furnas Formation has been duplicated along steep to shallowly dipping reverse fault zones. In a SW-NE section (Fig. 6b), we observed that meter-scale slices of fine grained sandstones of upper Furnas Formation were juxtaposed with basal Furnas conglomerate along NE-dipping reverse faults. The orientation of the fault zones is consistent with the inward movement of the sediments during central uplift formation. A detailed kinematic analysis of the block movement is difficult because much of the core-collar contact is covered by impact related breccias (Fig. 6b).

Beyond the 500 m wide megablock zone, the sediments of the Furnas Formation show consistent (albeit complex) bedding orientations as a result of cohesive deformation. This is particularly true for the upper part of the formation, which is well exposed on several 2–6 km long ridges around the core of the central uplift (Fig. 6a). Two ridges in the northern, northeastern and northwestern sectors of the collar show a

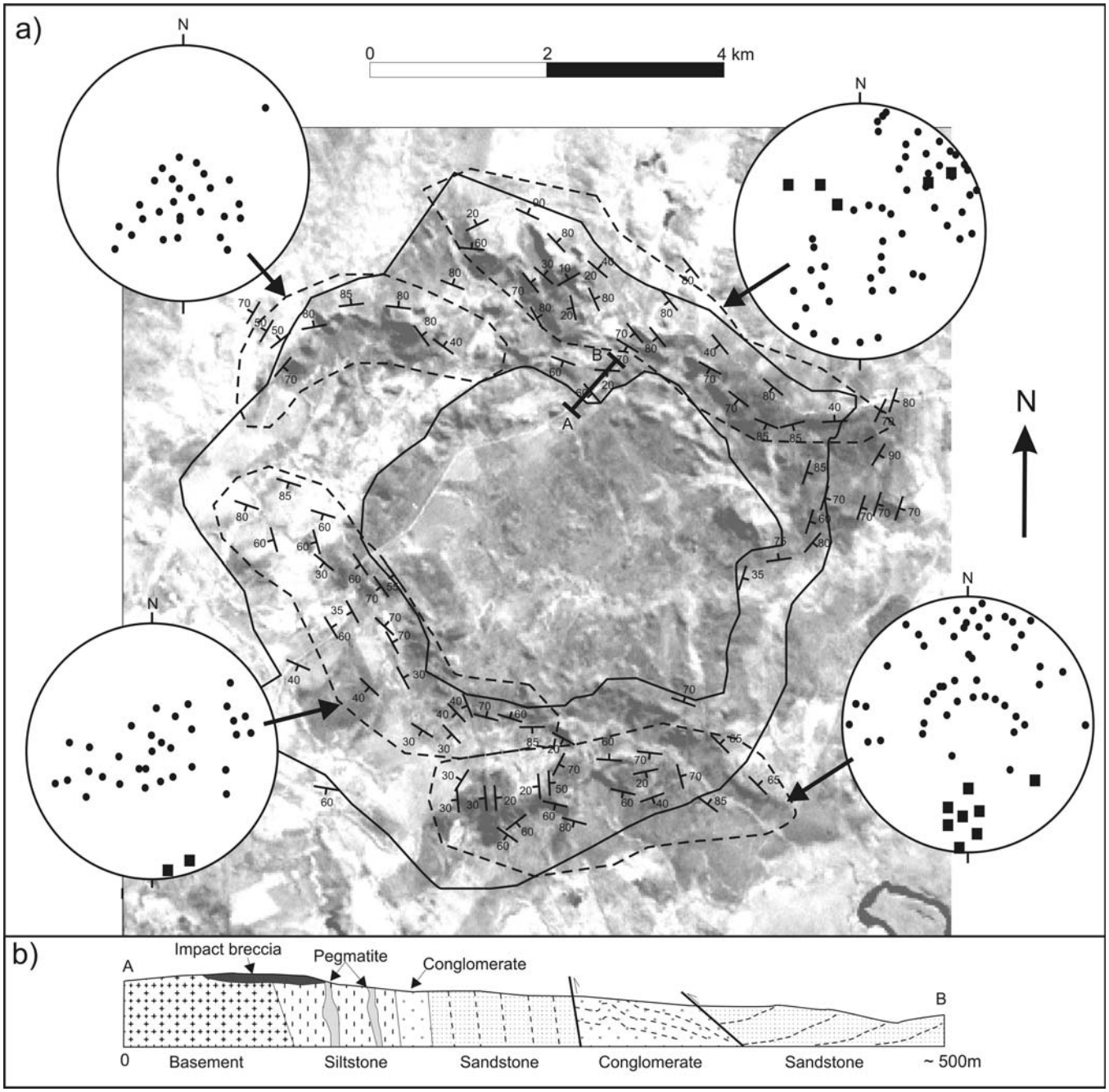


Fig. 6. a) Structural map of the collar of the Araguainha central peak. Lower hemisphere equal area projections indicate pole to the bedding (circles) for individual structural domains of the core. Black squares in stereonet projections indicate fold hinges. b) Structural profile showing the structural arrangement of the lithologies at the contact between the crystalline core and the collar sediments. The orientation of the profile is labeled in Fig. 6a.

prominent sigmoidal (Z-shape) geometry. The longest ridge spans 6 km from the northern to northeastern sector of the central peak, but has been segmented by a number of radial to oblique fault zones. The overall orientation of the Furnas bedding is roughly parallel to the NW-SE trend of the ridge (Fig. 7a). The strata dip steeply NE or are overturned (dipping 40–70 SW) along some segments of the ridge. The bedding has been deformed into hundred-meter scale gentle folds that plunge gently to the NW (Fig. 7b). These folds are similar in many aspects to radial gentle folds observed in the collar of the Vredefort Dome (Wieland et al. 2005), and are probably associated with buckling and thickening of the Furnas Formation. In addition, several outcrop-scale folds (ranging from vertically plunging recumbent to shallowly NW plunging isoclinal folds; Figs. 7c and 7d) indicate that slip movement between the strata contributed to further thickening of the

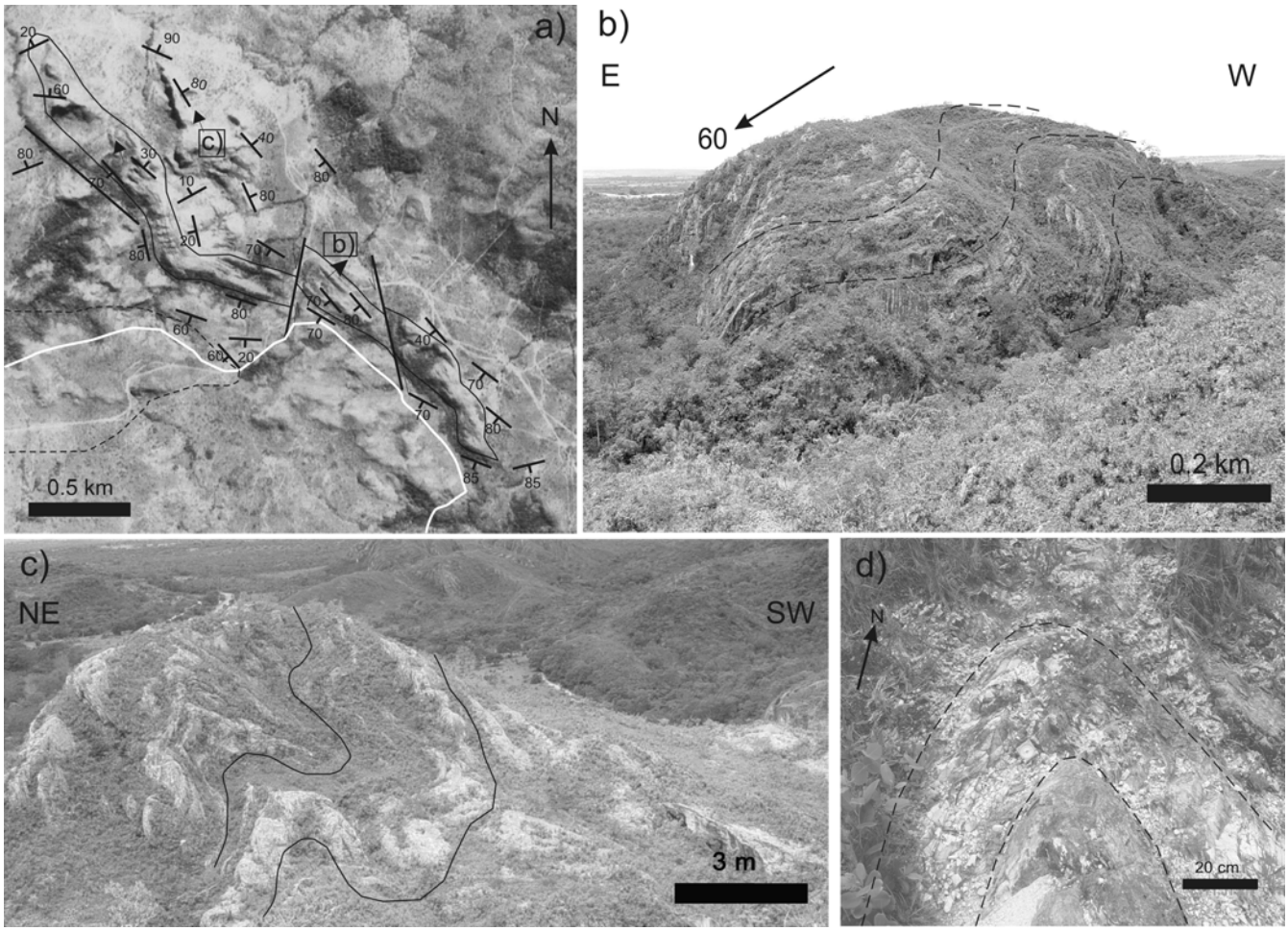


Fig. 7. a) Detail of bedding orientations in the sandstone ridge of the northeastern sector. The bridge has been separated into several segments by radial faults. White line marks core-collar contact. b) Example of outward plunging radial fold in the Furnas sandstones. The fold plunges 60 NE. c–d) Example of steeply NW plunging intrafolial folds in the Furnas sandstones. The folds range from recumbent (c) to isoclinal (d).

strata. The ridge in the northwestern sector is 2 km long and exposes upright to steeply outward dipping Furnas sandstones. Bedding in the sandstone changes from an east-west trend (tangential to the core-collar contact) to a NNE trend near the contact with the Ponta Grossa Formation. Much of the local variation in bedding orientation relates to fault-related block tilting between fault segments. No visible outcrop-scale folds or extreme variation of bedding have been observed, indicating a less complex deformation pattern in the northwestern sector relative to that of the northern and northeastern sector.

The arrangement of the strata in the southwestern sector follows a similar sigmoidal pattern to that described above. Although there is no prominent ridge in this sector, the sigmoidal (Z-shaped) pattern can be traced along a large number of scattered outcrops from the south to the west along the core-collar contact (Fig. 6a). The strata change from a NW-SE trend (parallel to the core-collar contact) to a WNW-ESE trend to the south and to the west. Small-scale folding could not be identified, but there is substantial evidence of overturned bedding (Fig. 5a) due to localized block tilting.

Abundant outcrops are found along an east-west trending ridge in the southern sector, which exposes the upper section of the Furnas Formation (Fig. 8a). The Furnas strata are steeply dipping, with much of the bedding dipping south, southeast or southwest (Figs. 8a and 8b). Along the southern face of the ridge, the strata dip 60–80 SW or SE. The slight variation in the overall bedding orientations (from south to southeast or southwest) relates to two main oblique faults that seem to represent conjugate sets of strike slip faults (Fig. 8a). Large-scale variation in the bedding orientation is also observed, with the beds tilted from subhorizontal to vertical due to large-scale folding of the strata. Local-scale variation also occurs due to outcrop-scale folding. The Furnas Formation has been largely folded into open to tight folds, with most of the fold axes plunging to variable degrees to the south (Fig. 8c). In addition, we have observed west-verging

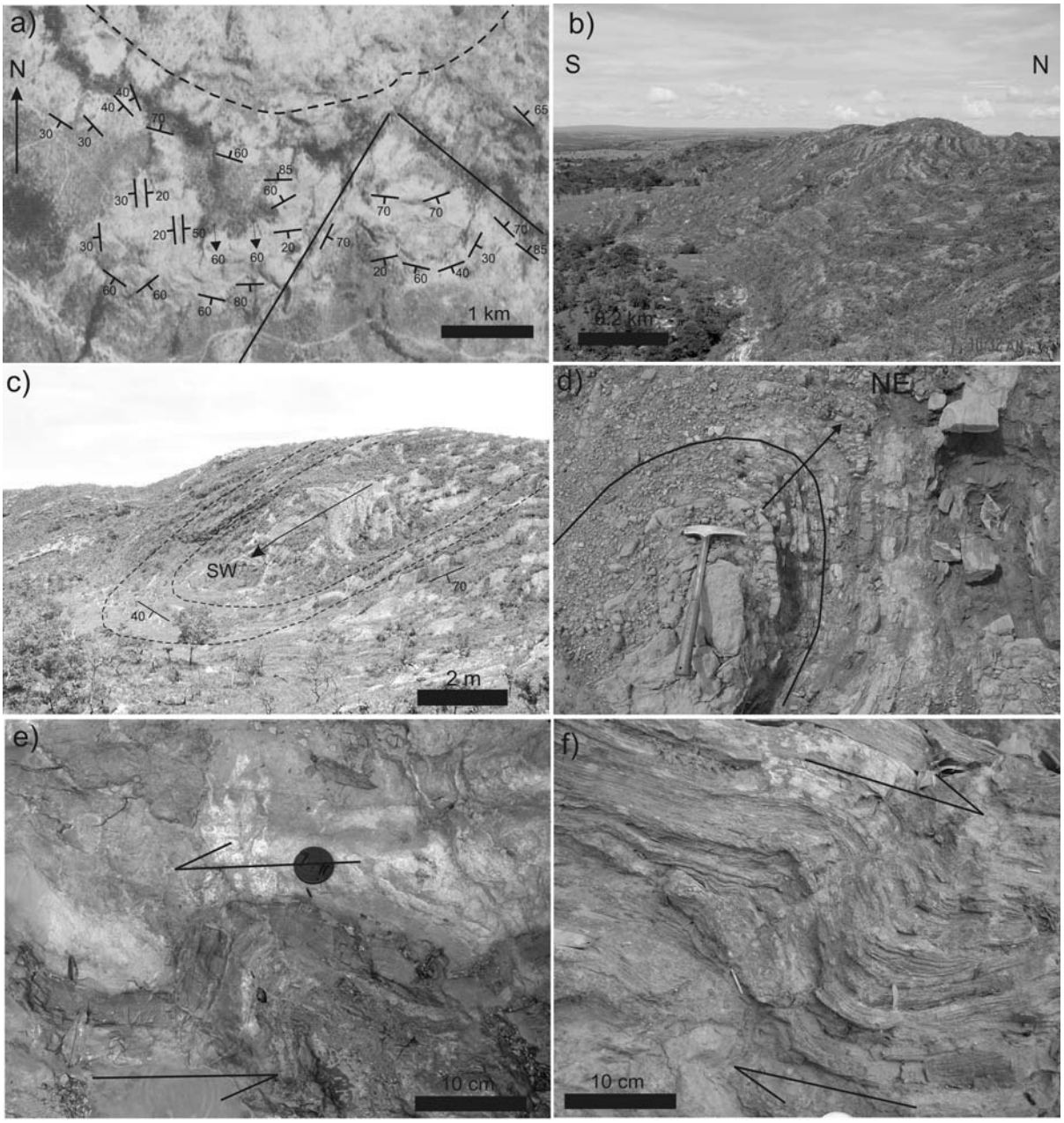


Fig. 8. a) Detail of bedding orientations in the sandstone ridge of the southern sector. b) Oblique view of the southern limb of the ridge shown in (a); note that the Furnas strata dip steeply to the south. c) View of the eastern side of the ridge where the Furnas strata are folded into a large-scale SW plunging fold (arrow points of the SW plunge; solid line shows bedding contour). d) Isoclinal NE plunging fold in the sediments of the Ponta Grossa Formation. e–f) Outward verging folds in the Ponta Grossa sediments. The fold geometry is consistent with movement of the Ponta Grossa towards the crater rim.

imbrication features, which together with the fold geometry and the conjugate nature of the faults, suggest an element of E-W compression, consistent with the tangential shortening of the strata during the central uplift formation.

While the ridges from all sectors expose the same upper section of the Furnas sandstones, they display different structural elements and seem to represent independent thrust sheets of the Furnas Formation. Evidence for repetition of the bedding and steep bedding orientations (e.g., between the ridges in the north and northwest) (Fig. 6) are a clear indication of large-scale imbrication of the km-scale sheets during the central uplift formation. In addition, the change in the strike of the bedding from concentric to oblique/tangential occurs in all individual ridges of the central uplift and may represent zones of convergence between the individual thrust sheets.

### The Annular Basin

Much of the annular basin is covered by Quaternary deposits and the relatively poor nature of the outcrops makes structural analysis difficult. The basin exposes dominantly iron-rich siltstones intercalated with fine-grained sandstone and occasional lenses of conglomerate of the Ponta Grossa Formation. Bedding orientation of the sediments varies from concentric to oblique with the concentrically disposed beds generally dipping outward at moderate angles. These beds may also have been folded into concentric open folds with upright geometries. Radial folds have also been observed; most of which have recumbent to isoclinal geometries (Fig. 8d) and fold hinges with seemingly random orientations. Locally, some of the concentrically arranged beds show cm-scale intrafolial folds with an asymmetric geometry that suggests outward movement of the upper sediments (Figs. 8e and 8f).

The Aquidauana Formation is well exposed in the northern sector of the annular basin, but is partly covered by Quaternary deposits in the south. The sediments are massive, with poorly developed bedding structures and layering. For most parts of the annular basin, the layering is defined by 0.5–2.0 m thick, massive sandstone alternating with 0.2–1.0 m thick conglomerate beds. Bedding becomes more prominent near the annular ring zone, and is arrayed concentrically around the basin, dipping shallowly to steeply inwards. It seems to describe small-scale shallow to tight folds, but transposition by faulting, intense fracturing and brecciation on a centimeter-scale do not allow a complete analysis of the fold geometries. Intense fracturing and localized brecciation of the Aquidauana Formation are common features elsewhere around the contact with the Ponta Grossa Formation.

## DISCUSSION

Impact craters ranging in size from a few kilometers to several tens or hundreds of kilometers have provided important information on the final stages of the impact cratering process (Wilshire et al. 1976; Roddy 1979; Shoemaker and Shoemaker 1996; Milton et al. 1996; Lana et al. 2003a, 2003b, 2006b; Wieland et al. 2005; Osinski and Spray 2005; Kenkmann et al. 2005). Structural analyses of small- to medium-sized complex structures (diameter between 2 and 25 km) have revealed a complex deformation history with lateral and vertical constriction of the target rocks during crater collapse (e.g., Wilshire et al. 1972; Roddy 1979; Shoemaker and Shoemaker 1996; Milton et al. 1996; Osinski and Spray 2005; Kenkmann et al. 2005; Scherler et al. 2006). Field-based structural studies in impact craters larger than 25 km are, however, limited and often directed at the evolution of their central uplift (e.g., Visnevsky and Montanari 1999; Lana et al. 2003a, 2003b, 2004; Wieland et al. 2005). The results of this study, which comprise the most complete structural data set for a 40 km wide impact structure, allow a direct evaluation of the process of transient cavity collapse and formation of the crater rim and the central uplift.

### Collapse of the Transient Cavity Walls

Observations at extraterrestrial craters indicate that formation of the crater rim is directly related to concomitant inward movement and downfaulting of the target rocks due to gravitational collapse of the transient cavity walls (e.g., Melosh 1989; Melosh and Ivanov 1998). Many extraterrestrial craters are characterized by scalloped rims, with slump terraces that stand above an otherwise flat interior floor. In contrast, terrestrial craters have been eroded and do not preserve their terraced walls. Their rims are often defined by fault-bounded blocks that slid down along radial and concentric faults during the transient cavity collapse (e.g., Wilshire et al. 1976; Milton et al. 1996; Reimold et al. 1998; Osinski and Spray 2005). The crater rim at Araguainha is to some extent comparable to the crater rim at the 23 km wide Haughton impact structure (Osinski and Spray 2005), where km-size blocks are bounded by radial and concentric faults, and the target rocks within individual blocks are variably folded.

For most parts of the Araguainha crater rim, the layered target strata are gently folded or may form shallowly dipping monoclines. The geometry of the gentle folds seems to be directly related to lateral compression and bulk shortening of sediments during collapse of the crater rim. We suggest that the gentle folding began during crater expansion or in crater collapse stage. This was then followed by the downfaulting of the target rocks and formation of km-scale blocks, which in all likelihood occurred while the inward lateral movement was in progress, during collapse of the transient cavity.

Estimates of the transient cavity dimensions at Araguainha (20–25 km wide and 2.0–2.5 km deep) (Engelhardt et al. 1992; Lana et al. 2006a, 2007) indicate that the crystalline basement rocks were exposed in a radius of several kilometers at the floor of the transient cavity and that much of the layered sedimentary rocks exposed in the collar of the central uplift have been detached from the walls of the transient cavity (e.g., Lana et al. 2006a). This implies that the target rocks of the cavity walls moved inward by several kilometers before they reached their present orientation in the crater floor and central uplift. A similar scenario has been shown by numerical modeling of the 12–16 km wide Sierra Madera impact structure (Goldin et al. 2006), where the sedimentary strata (overlying the Hess Formation; Wilshire et al. 1976) were thinned to almost nothing at the floor of the transient cavity. The final result of this numerical modeling appears to indicate substantial lateral movement of the sedimentary target from the transient cavity walls to the

central uplift (Goldin et al. 2006). An important question that remains is the nature of strain that accommodate the inward movement of target rocks during transient cavity collapse.

Compilation of structural data led Kenkmann (2002) to suggest that the inward movement of the target rocks in small- to medium-size impact craters may be accommodated by several listric faults that merge into low-angle (horizontal) detachments in the crater floor. However, our observation at Araguainha and recent structural observations and seismic data from the Haughton structure (Osinski and Spray 2005) do not indicate the large-scale inward movement along low-angle detachment zones. In addition, warping of normal listric faults and formation of low-angle detachments require specific geothermal gradient changes and/or variations of the stress field (e.g., Davis and Lister 1988; Melosh 1990; Parsons and Thompson 1993; Coleman and Walker 1994), which may not be entirely consistent with the extremely fast strain rates of the impact process.

The large number of asymmetric folds and the network of bedding parallel cataclastic breccia veins along the Araguainha rim (Figs. 3d and 4f), as well as the kilometer-scale anticline in the outer ring (Fig. 5a), suggest that the nature of strain related to the transient cavity collapse was more evenly distributed during inward movement of the target rocks, rather than focussed in a detachment fault. The large-scale inward motion of the sediments is accounted for by the asymmetric folds in the Passa Dois sequence and the inward-verging geometry of the outer anticline (Fig. 5a). These folds structures suggest that at least part of the deformation was non-coaxial within individual layers of the Aquidauana sequence, and that the topmost sediments moved inwards, towards the central parts of the structure. We suggest that inward movement recorded at the present level of erosion was mainly accommodated by differential slip between the strata, which in turn led to folding in the Passa Dois and Aquidaunha sediments. The fact that the Aquidauana Formation was folded into km-scale anticlines and that similar concentric features are present in the basement rocks (e.g., Schnegg and Fontes 2002) may also indicate that the bulk of the deformation was distributed not only through the sedimentary sequence but also into the underlying basement rocks, thus precluding the need for large-magnitude detachment faults.

Distribution of strain and non-coaxial deformation in mixed target rocks have also been predicted by numerical modeling of several impact structures (e.g., Collins and Wünnemann 2005; Wünnemann et al. 2005; Goldin et al. 2006). Numerical modeling of the Chesapeake Bay impact structure (Collins and Wünnemann 2005) is particularly relevant to our observations because it demonstrates the heterogeneous nature of strain in the outer part of the structure, and also shows how some individual layers could have been folded by non-coaxial deformation during the inward movement of the target rocks (see tracer lines in Figs. 2 and 3 in Collins and Wünnemann 2005). More importantly, the tracer lines depicted in the Collins and Wünnemann's (2005) model describe folds with similar geometry and magnitude (hundreds of meters) to the outer anticline at Araguainha and may indicate that the strain related to inward collapse of transient cavities can be quite evenly distributed through the target strata.

The close association of dykes and veins of cataclastic breccia with the folds in the Araguainha crater rim is directly related to the inward movement of the target rocks. Previous observations have suggested that networks of breccia can accommodate the instantaneous folding during collapse of complex craters (Kenkmann 2002; Lana et al. 2003a, 2006b; Wieland et al. 2006). According to these studies, the presence of a pervasive network of fractures and breccias may have provided the necessary temporary strength degradation for folding of the strata during the inward movement of the target rocks. Although there is no evidence of large slip magnitudes along major dykes of breccia, the consistent mm- to cm-scale displacements of the bedding along the veins suggest that the high-strain deformation could have been distributed as discrete shear in the breccia-fracture network.

**Formation and Collapse of the Central Uplift**

Previous studies at the Araguainha central uplift made a case that the kilometer-scale vertical exhumation of the granitic rocks in the core was accompanied by thickening of the Furnas and Ponta Grossa Formations in the collar (e.g., Lana et al. 2006a; 2007). The observations presented here indicate that thickening of the Furnas Formation was heterogeneous and partitioned between the individual ridges of the Furnas Formation. This in turn led to an asymmetric geometry of the central uplift, with the collar being substantially thicker in the western sector relative to the eastern sector (e.g., Lana et al. 2007). The cause of the asymmetric distribution of the individual ridges around the core of central peak is not well understood, and whether this fact might reflect strain partitioning related to an oblique impact (as suggested for other asymmetric central peaks, Scherler et al. 2006) or to pre-existing heterogeneities in the target sequence must remain speculative.

Less speculative is the assertion that thickening of the collar strata was due to progressive deformation, during the lateral movement of the target rocks—from the transient cavity walls to the central part of the crater. We observed that the target rocks followed four main stages of deformation before they finally reached their present upright to overturned orientation in the collar:

- *Outcrop-scale folding as a result of differential slip movement between strata.* Isoclinal folds (Figs. 7c and 7d) have contributed to target thickening in each of the individual ridges (or sheets) of the Furnas Formation.

This process might have began early in the collapse stage, with the inward movement of the target rocks from the transient cavity walls to the central uplift.

- *Imbrication of km-scale sheets of Furnas strata.* The structural stacking of distinct sheets resulted in the duplication of the stratigraphy in several sectors of the collar of the central uplift. The stacking was also responsible for the present sigmoidal pattern of bedding orientations (Fig. 6). Similar arrangement of sheets of target rocks has been observed in several other impact structures, and seems to be a common structural process during central uplift formation (e.g., Wilshire et al. 1976; Kenkmann et al. 2005; Scherler et al. 2006).
- *Lateral constriction of the sediments.* The constriction of the sediments led to formation of radially outward plunging gentle folds. Radially plunging folds have been observed in central uplifts of different sizes (Wilshire et al. 1976; Milton et al. 1996; Kenkmann et al. 2005; Osinski and Spray 2005; Wieland et al. 2005) and seem to accommodate much of the constrictional strain created by the inward movement of the target rocks during transient cavity collapse. At Araguainha, these folds might have contributed to further thickening of the strata during or shortly after thrust-related imbrication of the large-scale sheets (Fig. 7b).
- *Additional rotation of the bedding due to continuous uplift of the crystalline basement rocks.* Although the structural stacking resulted in the reorientation of the structural features, the mechanics of thrusting alone would not count for the subvertical, vertical, and locally overturned orientations of the Furnas strata. We believe that additional rotation of the bedding to vertical orientations might have been associated with progressed uplift of the crystalline core to its maximum height.

The surrounding Ponta Grossa sediments have been thickened by factors of 2 to 4 (Lana et al. 2007) and have been uplifted by more than 1 km during the central uplift formation. It is possible that these sediments record a similar structural evolution to that described above, but the poor exposure does not allow a complete reconstruction of the target rock movement. The steep orientation of the sediments and the orientation of isoclinal folds (e.g., Fig. 8d) in the Ponta Grossa sediments suggest that at least part of the strain field was compressional. Further complications in the structure of the Ponta Grossa Formation (e.g., fold hinges with random orientations) should be attributed to the fact that central uplifts of medium- to large-size complex structures are expected to collapse outward (e.g., Collins et al. 2002; Lana et al. 2003a, 2006b; Osinski and Spray 2005; Wieland et al. 2005; Wünnemann et al. 2005). Kinematic features indicating how the central uplift has collapsed are rare, possibly because the deformation would not be substantially coherent to form ductile asymmetric structures (e.g., Wieland et al. 2005). Direct evidence of the central uplift collapse with outward movement of the Ponta Grossa sediments is only indicated by the presence of small-scale outward-verging intrafolial folds (Figs. 8e and 8f). The geometry of these folds suggests that outer parts of the Ponta Grossa slipped toward the crater rim.

According to numerical models by Collins et al. (2002), the outward collapse of central uplift creates a centrifugal flow field that overrides the centripetal flow that departs from the collapsing cavity walls. The interaction between the two flow fields generates the circular topographic ring surrounding a central basin. We suggest that the inner ring feature at Araguainha is an expression of these opposite flow fields. The Araguainha inner ring exposes strongly faulted and fractured basal sandstones of the Aquidauana Formation, and it is likely that these sediments have been rotated from their original horizontal orientation and uplifted by hundreds of meters (Figs. 2b and 2c). The degree of rotation (up to subvertical attitudes) and uplift of the sediments can only be reconciled with compressional strains caused by the concomitant collapse of the central uplift and transient cavity walls. This implies that at a radial distance of 14 km from the centre of the structure and at the present level of exposure the target rocks may have been affected by far-field stresses related to the collapse of the central uplift.

## CONCLUSIONS

Detailed structural analysis at the Araguainha impact structure has provided important constraints on the collapse of its transient cavity. Collapse of the Araguainha cavity was accompanied by formation of large-scale fault-bounded blocks, which are now concentrically arranged around the rim of the impact structure. The blocks have been formed by semi-contemporaneous radial and concentric faulting that shaped much of the geometry, morphology, and structure of the crater rim. Sediments in the individual blocks record an early history of folding that predates much of the radial and concentric faulting. The inward-verging geometry of the folds is consistent with differential slip movement between the strata that might have been initiated during the early stages of transient cavity collapse. The bulk of the strain related to the collapse of the transient cavity wall was, thus, partitioned between differential slip (bedding parallel) movement and radial and concentric faulting. No evidence for low-angle detachment faults has been observed at the present level of erosion.

The formation of the central uplift was associated with large-scale upward movement of the crystalline basement and inward moment of the sedimentary target rocks. The sediments comprising the collar of the central uplift were most likely displaced from the transient cavity walls. The inward movement from the cavity walls to the collar of the uplift resulted in extreme thickening of the target rocks. The thickening involved: 1) isoclinal folding as a result of

differential slip movement between strata, 2) imbrication of km-scale thrust sheets of the Furnas strata, and 3) formation of radial folds during lateral constriction of the sediments. Much of the bedding orientation presently observed in the collar of the central uplift relates to the imbrications of the km-scale thrust sheets. Additional rotation of the bedding to their vertical orientations was caused by progressed uplift of the crystalline basement rocks.

The deformation in the annular trough of the crater (including formation of the ring features) was initiated during the collapse of the central uplift and transient cavity walls. The collapse of the central uplift was probably accompanied by formation of inclined folds in the Ponta Grossa Formation (in the collar of the central uplift) and excessive rotation and stratigraphic uplift of the sediments in the inner ring feature. The inner ring, which possibly represents a concentric anticline, marks the extent of deformation related to the outward movement of the target rocks. In contrast, formation of the outer anticline is associated with the differential movement of the target rocks during the collapse of the transient cavity walls. The last stage of deformation is marked by radial faults that displaced the outer ring feature and the crater rim by a few kilometers.

*Acknowledgments*—This project was funded by the São Paulo State Science Foundation (FAPESP) through research grant No. 05/51530-3. Cristiano Lana acknowledges support from the Barringer Family Fund for Impact Cratering Research and the Claude Leon Foundation of South Africa. Reviews by referees Gordon Osinski and Thomas Kenkmann, and associate editor John Spray were greatly appreciated.

*Editorial Handling*—Dr. John Spray

## REFERENCES

Bischoff L. and Prinz T. 1994. Der Araguainha-Krater (Brasilien): Das geologische Bild einer großen Impaktstruktur nach Geländebefunden und Satellitenbildanalyse. *Geowissenschaften* 12:5–14.

Coleman D. S. and Walker J. D. 1994. Modes of tilting during extensional core complex development. *Science* 263:215–218.

Collins G. S. and Wünnemann K. 2005. How big was the Chesapeake Bay impact: Insights from numerical modeling. *Geology* 33:925–928.

Collins G. S., Melosh H. J., Morgan J., and Warner M. 2002. Hydrocode simulations of Chicxulub crater collapse and peak-ring formation. *Icarus* 157:24–33.

Collins G. S., Melosh H. J., and Ivanov B. A. 2004. Modeling damage and deformation in impact simulations. *Meteoritics & Planetary Science* 39:217–231.

Crósta A. P., Gaspar J. C., and Candia M. A. F. 1981. Feições de metamorfismo de impacto no Domo de Araguainha. *Revista Brasileira de Geociencias* 11:139–146.

Davis G. A. and Lister G. S. 1988. Detachment faulting in continental extension: Perspectives from the southwestern U.S. Cordillera. In *Processes in continental lithospheric deformation,* edited by Clark S. P., Burchfiel B. C., and Suppe J. GSA Special Paper 218. Washington, D.C.: Geological Society of America. pp. 133–159.

Dence M., Innes M., and Robertson P. 1968. Recent geological and geophysical studies of Canadian craters. In *Shock metamorphism of natural materials*, edited by French B. and Short N. Baltimore: Mono Book Corp. pp. 169–184.

Dence M. R. 2004. Structural evidence from shock metamorphism in simple and complex impact craters: Linking observations to theory. *Meteoritics & Planetary Science* 39:267–286.

Dypvik H. and Jansa L. 2003. Sedimentary signatures and processes during marine bolide impacts: A review. *Sedimentary Geology* 161:308–341.

Engelhardt W., Matthai S., and Walzebuck J. 1992. Araguainha impact crater, Brazil. I: The interior part of the uplift. *Meteoritics & Planetary Science* 27:442–457.

Gibson R. L. and Reimold W. U. 2005. Shock pressure distribution in the Vredefort impact structure, South Africa. In *Large meteorite impacts III,* edited by Kenkmann T., Hörz F., and Deutsch, A. Washington, D.C.: Geological Society of America, Special Paper 384. pp. 329–349.

Grieve R. A. 1987. Terrestrial impact structures. *Annual Review of Earth and Planetary Sciences* 15:245–270.

Grieve R. A. F. and Therriault A. 2000. Vredefort, Sudbury, Chicxulub: Three of a kind? *Annual Review of Earth and Planetary Sciences* 28:305–338.

Grieve R. A. F. and Therriault A. 2004. Observation at terrestrial impact structures: Their utility in constraining crater formation. *Meteoritics & Planetary Science* 39:199–216.

Grieve R. A. F., Robertson P. B., and Dence M. 1981. Constraints on the formation of ring impact structures, based on terrestrial data. In *Multi-ring basins: Formation and evolution,* edited by Schultz P. H. and Merrill R. B. New York: Pergamon. pp. 791–814.

Goldin T. J., Wünnemann K., Melosh H. J., and Collins G. 2006. Hydrocode modeling of the Sierra Madera impact structure. *Meteoritics & Planetary Sciences* 41:1947–1958.

Hartmann W. K. 1972. Interplanetary variations in scale of crater morphology—Earth, Mars, Moon. *Icarus* 17:707–713.

Hammerschmidt K. and Engelhardt W. 1995. Ar/Ar dating of the Araguainha impact structure, Mato Grosso, Brazil. *Meteoritics & Planetary Science* 30:227–233.

Ivanov B. A. and Deutsch A. 1999. Sudbury impact event: Cratering mechanics and thermal history. In *Large meteorite impacts and planetary evolution II*, edited by Dressler B. O., and Sharpton V. L. GSA Special Paper 339. Washington, D.C.: Geological Society of America. pp. 389–397.

Jansa L. F., Pe-Piper G., Robertson B., Friedenreich O. 1989. Montagnais: A submarine impact structure on the Scotian Shelf, eastern Canada. *Geological Society of America Bulletin* 101: 450–463.

Kenkmann T. 2002. Folding within seconds. *Geology* 30:231–234.

Kenkmann T. and Dalwigk I. 2000. Radial transpression ridges: A new structural feature of complex impact craters. *Meteoritics & Planetary Science* 35:1189–1201.

Kenkmann T., Jahn A., Scherler D., and Ivanov B. 2005. Structure and formation of a central uplift: A case study of at the Upheaval Dome impact crater, Utah. In *Large meteorite impacts III,* edited by Kenkmann T., Hörz F., and Deutsch A. GSA Special Paper 384. Washington, D.C.: Geological Society of America. pp. 85–115.

Lana C., Gibson R. L., and Reimold W. U. 2003a. Impact tectonics in the core of the Vredefort Dome: Implications for formation of central uplift in large impact structures. *Meteoritics & Planetary Science* 38:1093–1107.

Lana C., Gibson R. L., Kisters A., and Reimold W. U. 2003b.

Archean crustal structure of the Kaapvaal craton, South Africa—Evidence from the Vredefort Dome. *Earth and Planetary Science Letters* 206:133–144.

Lana C., Romano R., Reimold W. U., and Hippertt J. 2006a. Collapse of large complex impact structures: Implications from the Araguainha impact structure. *Geology* 34:9–12.

Lana C., Gibson R. L., Reimold W. U. 2006b. The Broodkop Shear Zone, southeastern Vredefort Dome, South Africa: A Dominion-related extensional collapse shear zone? *South African Journal of Geology* 109:265–278.

Lana C., Souza-Filho C., Marangoni Y., Yokoyama E., Trindade R., Tohver E., and Reimold W. U. 2007. Insights into the morphology, geometry and post-impact erosion of the Araguainha peak-ring structure, central Brazil. *Geological Society of America Bulletin* 119:1135–1150.

Masero W., Schnegg P. A., and Fontes S. L. 1994. A magnetotelluric investigation of the Araguainha impact structure in Mato Grosso-Goiás, central Brazil. *Geophysical Journal International* 116: 366–376.

Melosh H. J. 1989. *Impact cratering: A geological process.* Oxford: Oxford University Press. 245 p.

Melosh J. 1990. Mechanical basis for low-angle normal faulting in the Basin and range province. *Nature* 343:331–335.

Melosh H. J. and Ivanov B. 1999. Impact crater collapse. *Annual Review of Earth and Planetary Sciences* 27:385–415.

Milton D. J., Glikson A. Y., and Brett R. 1996. Gosses Bluff—A latest Jurassic impact structure, central Australia. Part 1: Geological structure, stratigraphy, and origin. *Journal of Australian Geology and Geophysics* 16:453–486.

Morgan J. V., Warner M. R., Collins G. S., Melosh H. J., and Christeson G. L. 2000. Peak ring formation in large impact craters. *Earth and Planetary Science Letters* 183:347–354.

Osinski G. R. and Spray J. G. 2005. Tectonics of the Haughton impact event, Devon Island, Canadian High Arctic. *Meteoritics & Planetary Science* 40:1813–1834.

Parsons T. and Thompson G. A. 1993. Does magmatism influence low-angle normal faulting? *Geology* 21:247–250.

Pena G. S. 1974. Geologia da Area do projeto Goiania II: Congresso Brasileiro de Geologia 28, Porto Alegre, Brazil. Sociedade Brasileira de Geologia. pp. 2–10.

Pike R. J. 1974. Depth/diameter relations of fresh lunar craters: Revision from spacecraft data. *Geophysics Research Letters* 1:291–294.

Pike R. J. 1977. Size-dependence in the shape of fresh impact craters on the moon. In *Impact and explosion cratering,* edited by Roddy D. J., Pepin R. O., and Merrill R. B. New York: Pergamon Press. pp. 489–509.

Pike R. J. 1983. Comment on a "A schematic model of crater modification by gravity" by H. J. Melosh. *Journal of Geophysical Research* 88:2500–2504.

Riller U. 2005. Structural characteristics of the Sudbury impact structure, Canada: Impact-induced versus orogenic deformation—A review. *Meteoritics & Planetary Science* 40: 1563–1752.

Reimold W. U., Brandt D., and Koeberl C. 1998. Detailed structural analysis of the rim of a large, complex impact crater: Bosumtwi crater, Ghana. *Geology* 26:543–546.

Roddy D. J. 1979. Structural deformation at Flynn Creek impact crater, Tennessee (abstract). 10th Lunar and Planetary Science Conference. pp. 2519–1534.

Romano R., Cooper G. R., and Reimold W. U. 2006. SRTM investigation of the Araguainha impact crater, central Brazil (abstract). *Meteoritics & Planetary Science* 41:A152.

Scherler D., Kenkmann T., and Jahn A. 2006. Structural record of an oblique impact. *Earth and Planetary Science Letters* 248: 28–38.

Schnegg P. A. and Fontes S. L. 2002. Feasibility study of the geoelectric structure of the Araguainha impact, Brazil. *Earth, Planets, and Space* 54:597–606.

Shoemaker E. M. and Shoemaker C. S. 1996. The Proterozoic impact record of Australia. *Journal of Australian Geology and Geophysics* 16:379–398.

Silveira Filho N. C. and Ribeiro C. L. 1973. Informacoes geologicas preliminares sobre a estrutura vulcanica de Araguainha: Relatorio Interno do Departamento Nacional de Pesquisas Minerais (DNPM). 50 p.

Spray J. G., Butler H. R., and Thompson L. M. 2004. Tectonic influences on the morphometry of the Sudbury impact structure: Implications for terrestrial cratering and modeling. *Meteoritics & Planetary Science* 39:287–301.

Theilen-Willige B. 1981. The Araguainha impact structure, central Brazil: *Revista Brasileira de Geociencias* 11:91–98.

Tsikalas F., Gudlaugsson S. T., Eldholm O., and Faleide J. I. 1998a. Integrated geophysical analysis supporting the impact origin of the Mjølnir structure, Barents Sea. *Tectonophysics* 289:257–280.

Tsikalas F., Gudlaugsson S. T., and Faleide J. I. 1998b. Collapse, infilling, and post-impact deformation at the Mjølnir impact structure, Barents Sea. *Geological Society of America Bulletin* 110:537–552.

Vermeesch P. M. and Morgan J. V. 2004. Chicxulub central crater structure: Initial results from physical property measurements and combined velocity and gravity modeling. *Meteoritics & Planetary Science* 39:1019–1034.

Vishnevsky S. and Montanari A. 1999. Popigai impact structure (Arctic Siberia, Russia): Geology, petrology, geochemistry, and geochronology of glass-bearing impactites. In *Large meteorite impacts and planetary evolution II,* edited by Dressler B. O. and Sharpton V. L. GSA Special Paper 339. Washington, D.C.: Geological Society of America. pp. 19–60.

Wieland F., Gibson R. L., and Reimold W. U. 2005. Structural analysis of the collar of the Vredefort Dome, South Africa—Significance for impact-related deformation and central uplift formation. *Meteoritics & Planetary Science* 40:1537–1554.

Wilshire H. G., Offield T. W., Howard K. A., and Cummings D. 1972. Geology of the Sierra Madera cryptoexplosion structure, Texas: USGS Professional Paper 599-H. 42 p.

Wünnemann K., Morgan J. V., and Jödicke H. 2005. Is Ries crater typical for its size? An analysis based upon old and new geophysical data and numerical modeling, In *Large meteorite impacts* III, edited by Kenkmann T., Hörz F., and Deutsch A. GSA Special Paper 384. Washington, D.C.: Geological Society of America. pp. 67–84.